

Polarization-insensitive complementary metamaterial structure based on graphene for independently tuning multiple transparency windows

Hailong Huang(黄海龙), Hui Xia(夏辉), Hongjian Li(李宏建)

Citation: Chin. Phys. B . 2020, 29(11): 114203 . **doi:** 10.1088/1674-1056/abb307
Journal homepage: http://cpb.iphy.ac.cn; http://iopscience.iop.org/cpb

What follows is a list of articles you may be interested in

An improved method for the investigation of high-order harmonic generation from graphene

Zhong Guan(管仲), Lu Liu(刘璐), Guo-Li Wang(王国利), Song-Feng Zhao(赵松峰), Zhi-Hong Jiao(焦志宏), Xiao-Xin Zhou(周效信)

Chin. Phys. B . 2020, 29(10): 104206 . **doi:** 10.1088/1674-1056/abab76

An ultrafast and low-power slow light tuning mechanism for compact aperture-coupled disk resonators

Bo-Yun Wang(王波云), Yue-Hong Zhu(朱月红), Jing Zhang(张静), Qing-Dong Zeng(曾庆栋), Jun Du(杜君), Tao Wang(王涛), Hua-Qing Yu(余华清)

Chin. Phys. B . 2020, 29(8): 084211 . **doi:** 10.1088/1674-1056/ab9df1

Low-power electro-optic phase modulator based on multilayer graphene/silicon nitride waveguide

Lanting Ji(姬兰婷), Wei Chen(陈威), Yang Gao(高阳), Yan Xu(许言), Chi Wu(吴锜), Xibin Wang(王希斌), Yunji Yi(衣云骥), Baohua Li(李宝华), Xiaoqiang Sun(孙小强), Daming Zhang(张大明)

Chin. Phys. B . 2020, 29(8): 084207 . **doi:** 10.1088/1674-1056/ab943b

A compact electro-absorption modulator based on graphene photonic crystal fiber

Guangwei Fu(付广伟), Ying Wang(王颖), Bilin Wang(王碧霖), Kaili Yang(杨凯丽), Xiaoyu Wang(王晓愚), Xinghu Fu(付兴虎), Wa Jin(金娃), Weihong Bi(毕卫红)

Chin. Phys. B . 2020, 29(3): 034209 . **doi:** 10.1088/1674-1056/ab6838

Generation of wide-bandwidth pulse with graphene saturable absorber based on tapered fiber

Ren-Li Zhang(张仁栗), Jun Wang(王俊), Mei-Song Liao(廖梅松), Xia Li(李夏), Pei-Wen Guan(关珮雯), Yin-Yao Liu(刘银垚), Yan Zhou(周延), Wei-Qing Gao(高伟清)

Chin. Phys. B . 2019, 28(3): 034203 . **doi:** 10.1088/1674-1056/28/3/034203

Polarization-insensitive complementary metamaterial structure based on graphene for independently tuning multiple transparency windows*

Hailong Huang(黄海龙)[1,2], Hui Xia(夏辉)[2], and Hongjian Li(李宏建)[2,†]

[1] The Research Department, Beijing Zhongkexin Electronics Equipment Co. Ltd, Beijing 101111, China
[2] School of Physics and Electronics, Central South University, Changsha 410083, China

(Received 24 May 2020; revised manuscript received 19 August 2020; accepted manuscript online 27 August 2020)

Polarization-insensitive multiple transparency windows are obtained with a graphene-based complementary metamaterial structure in terahertz regions, which is composed of two kinds of monolayer graphene perforated in shapes of a cross and four identical split rings that construct a resonator. The geometric parameters of resonators are different from each other. Numerical and theoretical results show that the quantum effect of Autler–Townes splitting is the key factor for appearance of transparency windows within the resonant dips. Further investigation demonstrates that by employing the fourfold-symmetry graphene complementary structure, polarization-independent transparency windows can be achieved. Moreover, multiple transparency windows can be separately manipulated over a broad frequency range via adjusting the chemical potential of the corresponding graphene resonators, and the bandwidth as well as resonance strength can also be tuned by changing the relative displacement between resonators each consisting of a cross and four split rings. The proposed metamaterial structure may be utilized in some practical applications with requirements of no polarization-varied loss and slowing the light speed.

Keywords: graphene, polarization-independent, multiple transparency windows

PACS: 42.79.Hp, 42.50.Gy **DOI:** 10.1088/1674-1056/abb307

1. Introduction

The well-known quantum effects of Autler–Townes splitting (ATS)[1] or electromagnetically induced transparency (EIT)[2–6] can generate transparency windows within two resonance dips, which have been utilized in many applications such as bio-sensors,[7] light slowing devices[8] and terahertz wave modulators.[9] Although the effects of ATS and EIT have similar transmission spectra, even some transformation would be happened between them under some situations,[10] their physical mechanisms are quite different.[11] Concerning about EIT, the destructive interference between two different excitation pathways can result in appearance of transparency windows, while in ATS it is caused by the strong coupling induced splitting of resonant modes. With geometric dimensions scaled down to micro- or nano-levels, a new concept of plasmon-induced transparency (PIT)[12] effect has been introduced to mimic EIT effect in microwave ranges and investigated in metamaterial (MM) structures to obtain transparency windows.

So far, working frequency bands of transparency windows observed in metal-based MM structures are fixed. Transparency windows can be tuned unless the geometric parameters or make-up constituents are re-optimized and re-selected. In practical applications, it is highly appreciated that transparency windows can be flexibly tuned without any variation in parameters or materials. Fortunately, some raw materials with tunable electromagnetic (EM) parameters (i.e., permittivity or permeability), such as phase-change materials,[13] ferrite-based materials[14] and nonlinear materials,[15] are found and used to achieve tunable properties. Especially graphene, a single layer of carbon atoms gathered in a shape of honeycomb lattice, is the best choice for achieving a tunable transparency window since it exhibits many unique physical properties and its response time is ultra-fast. Specifically, the tunable property has been obtained by varying the chemical potential of graphene material via chemical doping or electrostatic gating, which is ranged from -1 eV to 1 eV.[16,17] Owing to combination of strong plasmonic response and extremely low loss, the working frequency band of graphene-based MM structure can be tuned over a broad range from the terahertz to infrared frequencies.

Recently, many scientists have discovered that multiple transparency windows in graphene-based MM structures are more advanced than a single transparency window.[18–22] Nevertheless, most of the multiple transparency windows face a common problem what can also be found in single transparency windows. Performance of an induced transparency window would be worse gradually and it even disappears when the polarization angle of incident light is shifted significantly. In our previous paper,[23] a polarization-independent transparency window has been realized using resonators each

*Project supported by the National Natural Science Foundation of China (Grant No. 61275174).
†Corresponding author. E-mail: lihj398@126.com
© 2020 Chinese Physical Society and IOP Publishing Ltd

consisting of a metallic cross and four identical metal split rings, i.e., split-ring resonators (SRRs), which are placed on the surface of a planar monolayer graphene, and the EIT-like effect induces transparency windows. Although polarization-independent transparency windows are achieved owing to the center symmetry, some defects in this graphene-based MM structure are found and summarized as follows: Firstly, only a single transparency window can be obtained. Secondly, the preparation process for metal-graphene metasurface is complicated and inconvenient for large-scale production. Lastly, the individual adjustment of the transparency window cannot be realized, which is an important merit for multiple transparency windows to expand its practical applications. Therefore, it is still important and urgent to design graphene-based MM structures with a simple fabrication process as well as realizing the individual modulation of multiple transparency windows.

In this paper, a polarization-independent graphene-based complementary MM structure is proposed to obtain multiple transparency windows in a terahertz region, whose top layer is composed of two kinds of monolayer graphene perforated in shapes of a cross and four identical split rings that construct a resonator. The geometric parameters of resonators are different from each other. By investigating the relative displacements between the cross and the SRRs, it is found that the transparency window is more likely induced by the quantum effect of ATS, not the well-known EIT-like effect, and the working frequency band of multiple transparency windows can be individually tuned by varying the chemical potential of corresponding graphene resonators. Moreover, the performance of multiple transparency windows is immune to any variation in polarization angles because of the center symmetry. The theoretical results reveal that the SRRs can involve two strongly coupling modes, proving the origin of multiple transparency windows in our proposed structure. Therefore, we believe that the proposed graphene-based MM structure can pave a new way for some applications such as slow-light devices and light switches.

2. Designed model and simulated method

A unit cell of the proposed MM structure is illustrated in Fig. 1(a). Two kinds of graphene complementary structure (GCS) arrays with different sizes and element numbers are placed on the quartz glass substrate. It is worth noting that two GCSs are perforated, each consisting of a cross and four identical split rings, which are the common structure of the graphene resonators.[23,24] The detailed fabrication process is shown in Figs. 1(b)–1(d). First, two planar graphene monolayers are separately etched by an electron beam into the forms of a cross and four identical split rings with different geometric parameters. Then, two metal electrodes are deposited, and contacted to ultra-thin metal ribbon pairs, respectively, which are used to connect two kinds of GCSs (G1 and G2) along the y-direction. Secondly, the ion gel is spinning on arrays of two kinds of GCSs. Finally, a transparency indium-tin-oxide (ITO) film is deposited on the ion gel layer acting as a top gate electrode, and two external gate voltages V_{g1} and V_{g2} are applied on the corresponding graphene layer to tune the chemical potential, as shown in Fig. 1(e). The relationship between chemical potential (E_f) and external gate voltage (V_g) is expressed as follows:[25]

$$E_{fi} = \hbar v_f \sqrt{\frac{\pi \varepsilon_s \varepsilon_0 V_{gi}}{e t_2}}, \quad (i = 1, 2) \tag{1}$$

where $v_f = 10^6$ m/s is the Fermi velocity, ε_s and t_2 are assigned as the quartz's relative permittivity and thickness, respectively, ε_0 is air permittivity, e is the electron charge, $\hbar$ is the reduced Planck constant.

In the terahertz regimes, graphene's surface conductivity is described by the Drude model[26]

$$\sigma_g = \frac{e^2 E_f}{\pi \hbar^2} \cdot \frac{\mathrm{i}}{\omega + \mathrm{i}\tau^{-1}}, \tag{2}$$

where $\tau = \mu E_f/(e v_f^2)$ is the carrier relaxation time related with a maximum electron mobility of $\mu = 200000\ \mathrm{cm^2 \cdot V^{-1} \cdot s^{-1}}$.[27] The relative permittivity of graphene is written as

$$\varepsilon(\omega) = 1 + \mathrm{i}\frac{\sigma_g}{t_g \varepsilon_0 \omega}. \tag{3}$$

Graphene can be modelled as an effective medium with the atom-like thickness of $t_g = 0.034$ nm. Hence, a practical device for the aim of independently manipulating the multiple transparency windows is obtained.

In order to obtain the numerical results, the three-dimensional electromagnetic simulation method based on finite integrated technology (FIT) is used to simulate the PIT effect.[28,29] During the simulation, the unit cell boundary conditions are applied at the x and y directions, while the transverse electric (TE) polarized wave is normally irradiated in the z direction with a perfectly matched layer. The thickness and index of the quartz glass are 40 nm and 3.75, respectively. The periodicity spacings of unit cells in the x and y directions are considered as $P_x = 600$ nm and $P_y = 1030$ nm. In the large-sized GCS (G1), the length of the cross is $L_1 = 300$ nm and its width is $W = 15$ nm. Four identical split rings have the outer radius of $R_1 = 50$ nm, width of $W_1 = 30$ nm and the gap width of $g_1 = 35$ nm. The relative distance between the center of the rings and adjacent bars of the cross is set as d_1, while the width of the large-sized GCS is $P = 500$ nm. In the small-sized GCS (G2), the length of the cross is $L_2 = 200$ nm and its width is $W = 15$ nm. The complementary rings have the outer radius $R_2 = 40$ nm, width $W_2 = 30$ nm and the gap width $g_2 = 20$ nm. The relative distance between the center of a ring and the adjacent bar of the cross is d_2, while the width of the small-size GCS is $P = 500$ nm.

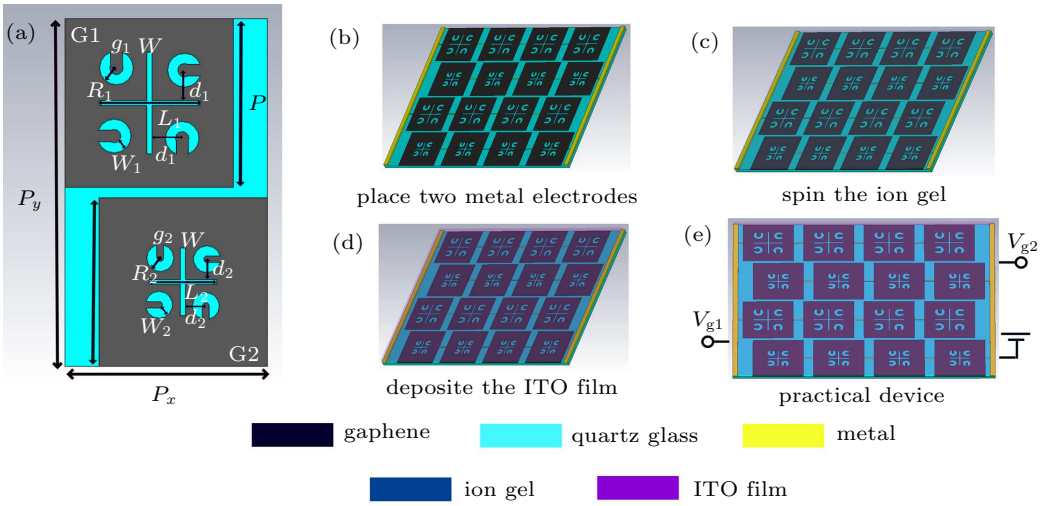


Fig. 1. (a) The photograph of the unit cell of multi-band PIT MM structure with the detailed geometric parameters. (b)–(d) The preparation process for controlling chemical potential of graphene resonators via the adjustable method of two top electrostatic grating. (e) The picture of a practical device.

3. Results and discussion

To dig out the origin of transparency windows in the GCSs, the transmission spectra of three graphene resonators with different sizes are initially plotted, as shown in Figs. 2(a) and 2(b). The first structure is designed with a monolayer graphene perforated with a cross, the second one is a monolayer graphene perforated with four identical split rings, and the third one is the combined GCS. In Fig. 2(a), it can be found that the resonant point of large-size cross structure is located at 13.68 THz, showing a typical LC resonant mode.[30] However, the large-size SRR structure has the weak resonance dip at 14.43 THz, which is caused by the dipole mode.[31] An obvious transparency window at 12.98 THz is appeared when the split rings and the cross are combined into one unit cell. From Fig. 2(b), the appearance of a transparency window in the small-size GCS can also be explained by the same way. Thus, the origin of the transparency window would be explained by the coupling effect between the cross and the split rings, which seems like that the transparency window is mainly induced by typical PIT effect, indicating the destructive interference between two weakly coupled modes. However, we think that the transparency window is more likely induced by the ATS effect instead of PIT effect,[32] and the cross plus four split rings structures should be treated as two strongly coupled modes with the similar quality factors (Q-factor).

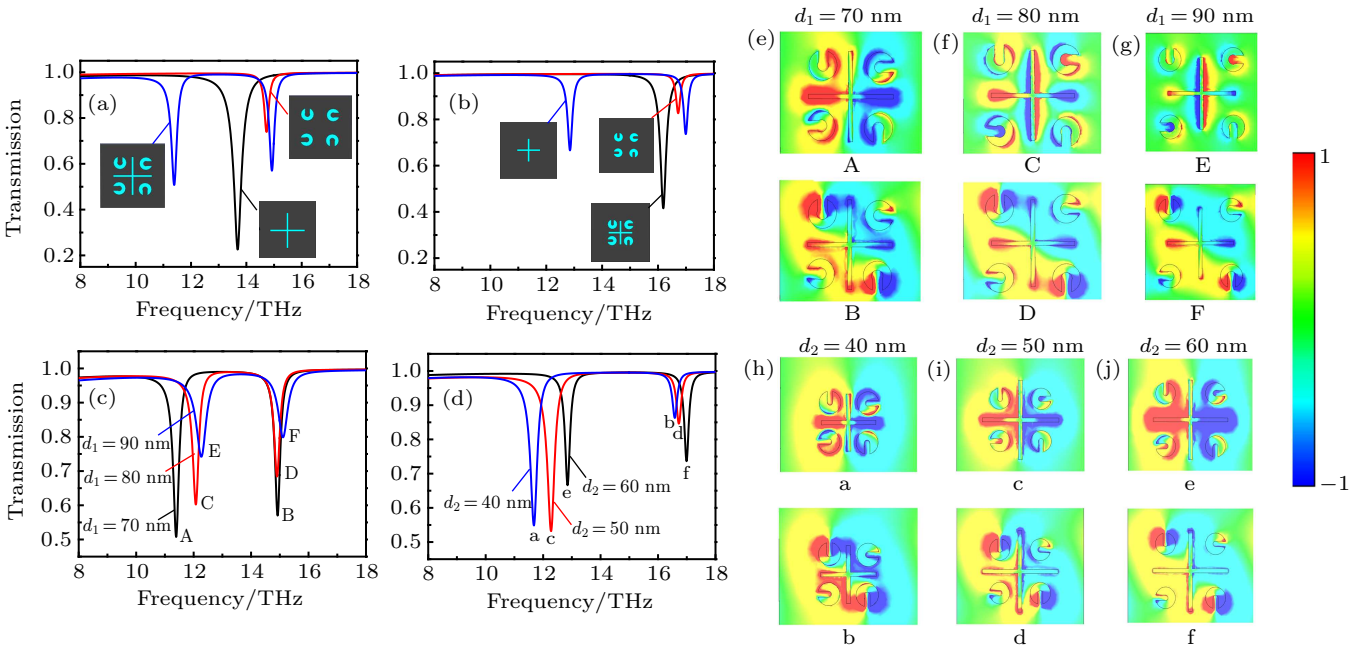


Fig. 2. Simulated transmission spectra of three graphene resonators: (a) large-size structure and (b) small-size structure. (c) and (d) Simulated transmission curves of G1 and G2 under different relative distances d_1 and d_2, respectively. (e)–(j) Z-component of magnetic field (H_z) of each transmission dip with normally incident wave.

To prove the above assumption about the origin of the transparency window, we investigated the effect of geometric parameters d_1 and d_2 on the transmission performance of GCSs in Figs. 2(c) and 2(d). Here, the separation between two transmission dips represents the coupling strength of two resonance structures. In Figs. 2(c) and 2(d), it is seen that with the increasing relative distance d_1 (or d_2), the separation between two transmission dips is decreased, indicating that the coupling strength between two resonance modes is decreased. An obvious transparency window will appear with the suitable relative distance d_1 (or d_2) between the SRRs and cross. The distribution of z-component magnetic fields (H_z) at different transmission dips are given in Figs. 2(e)–2(j). From Figs. 2(e)–2(g), it can be seen that the H_z distributions at each transmission dip is quite similar except intensity difference, revealing that two strongly coupled modes are induced by the same quantum effect. In the case of $d_1 = 70$ nm and 80 nm, the center of the SRRs is much closer to the cross than that of $d_1 = 90$ nm, and having much stronger magnetic field than that of $d_1 = 90$ nm. In other words, the coupling strength between the cross and the rings is affected by the geometric parameter d_1. Likewise, in the case of the small-size GCS, the similar H_z distributions and intensity difference are both observed in Figs. 2(h)–2(j). Based on the above analysis, the cross plus four-ring structures could be regarded as two oscillators with similar Q-factor, demonstrating the fact that the origin of transparency window is more likely caused by the quantum effect of ATS not the PIT effect.

In order to obtain the multiple transparency windows, two kinds of GCSs with different parameters and element numbers are designed and simulated with different displacements between the cross bar and the nearby rings, while the chemical potentials of the corresponding G1 and G2 are both fixed at 0.2 eV. In Fig. 3, it is clearly observed that multiple transparency windows are achieved at two frequencies of 11.62 THz and 15.45 THz, respectively. From Figs. 3(a)–3(d), we find that the separation between two transmission dips caused by the large GCS is decreased gradually when the relative distance d_1 is increased from 90 nm to 120 nm, while the distance $d_2 = 60$ nm is kept unchanged. Similarly, as shown in Figs. 3(e)–3(h), the effect of distance d_2 on transmission performance is investigated. It is seen that the separation between two transmission dips, which is caused by small-size GCS part, is also decreased with the relative distance d_2 increasing from 60 nm to 90 nm for the distance d_1 fixed at 90 nm. The H_z distributions of the combined structure at the transmission dip for $d_1 = 90$ nm ($d_2 = 60$ nm) and $d_1 = 120$ nm ($d_2 = 60$ nm) are plotted in Figs. 3(i) and 3(j), respectively; the transmission dip for $d_2 = 60$ nm ($d_2 = 90$ nm) and $d_2 = 90$ nm ($d_1 = 90$ nm) are plotted in Figs. 3(i) and 3(k), respectively. It is clearly seen that the resonant modes at the transmission dips for different d_1 or d_2 have similar H_z distributions in regardless of the intensity difference, which shows that this resonance comes from the same origin. In addition, the closer the two resonators are, the stronger the resonant mode is, and the multiple transparency windows remain unchanged. The similar physical phenomena can also be found in another paper.[33] Hence, with the appropriate displacements d_1 and d_2, multiple transparency windows can be obtained with the proposed MM structure.

The individual modulation of multiple transparency windows is vital in some applications where only a desired frequency band will be selected to meet the practical requirements, expanding the range of potential applications. By changing the chemical potential of the corresponding GCS part (E_{f1} and E_{f2}) via controlling the external gate voltages (V_{g1} and V_{g2}), the individual modulation is carried out. Noting that two relative displacements d_1 and d_2 between the cross and the rings are fixed at 90 nm and 60 nm, respectively. First, we simulate the transmission spectrum as a function of frequency when the chemical potential E_{f1} is varied from 0.19 eV to 0.22 eV while E_{f2} is fixed at 0.2 eV, as shown in Fig. 4(a). It is observed that the peak frequencies of two transmission dip 1/dip 3 are blue-shifted from 10.16 THz/14.07 THz to 11.18 THz/14.93 THz, while the transmission dip 2/dip4 are nearly fixed at 12.62 THz/16.48 THz. Thus, the transmission for $E_{f1} = 0.19$ eV and $E_{f1} = 0.22$ eV at 10.91 THz are 0.551 and 0.991, respectively, which indicates that the transmission could be switched between 55.1% and 99.1% by simply varying E_{f1} with a variation of 0.03 eV. Thus, a transmission magnitude modulation depth of 44.3% could be achieved via a small variation of 0.03 eV. Similarly, the transmission performance is then simulated with the chemical potential E_{f2} varying from 0.19 eV to 0.22 eV, while maintaining the E_{f1} is fixed at 0.2 eV, as shown in Fig. 4(b). It is noted that the peak frequencies of the transmission dip 2/dip 4 are blue-shifted from 12.36 THz/16.19 THz to 12.99 THz/17.25 THz, while the transmission dip 1/dip 3 are fixed at the frequencies of 10.86 THz/14.42 THz. Also, the transmission at 12.34 THz can be changed from 0.651 to 0.987 with a variation of 0.03 eV, indicating that a transmission magnitude modulation depth of 34.0% is obtained with a small variation of 0.03 eV. Interestingly, the transmission performance of multiple transparency windows experiences a very slight variation during the modulating process. Therefore, multiple transparency windows in the proposed MM structure can be modulated independently via adjusting the chemical potential of corresponding GCS part. Based on the above results, switches or modulators can be proposed to adjust the transmission magnitude at the resonance point. In Figs. 4(c) and 4(d), we further investigate the corresponding group delays for the proposed MM structure at different graphene's chemical potentials. Positive and negative values refer to the slow and fast light, respectively. From Figs. 4(c) and 4(d), we can see that a

positive group delay of 0.6 ps is obtained in the vicinity of the corresponding transmission peak, indicating a slow light effect. Also, the group delays are tuned individually with different chemical potentials, covering multiple frequency regions.

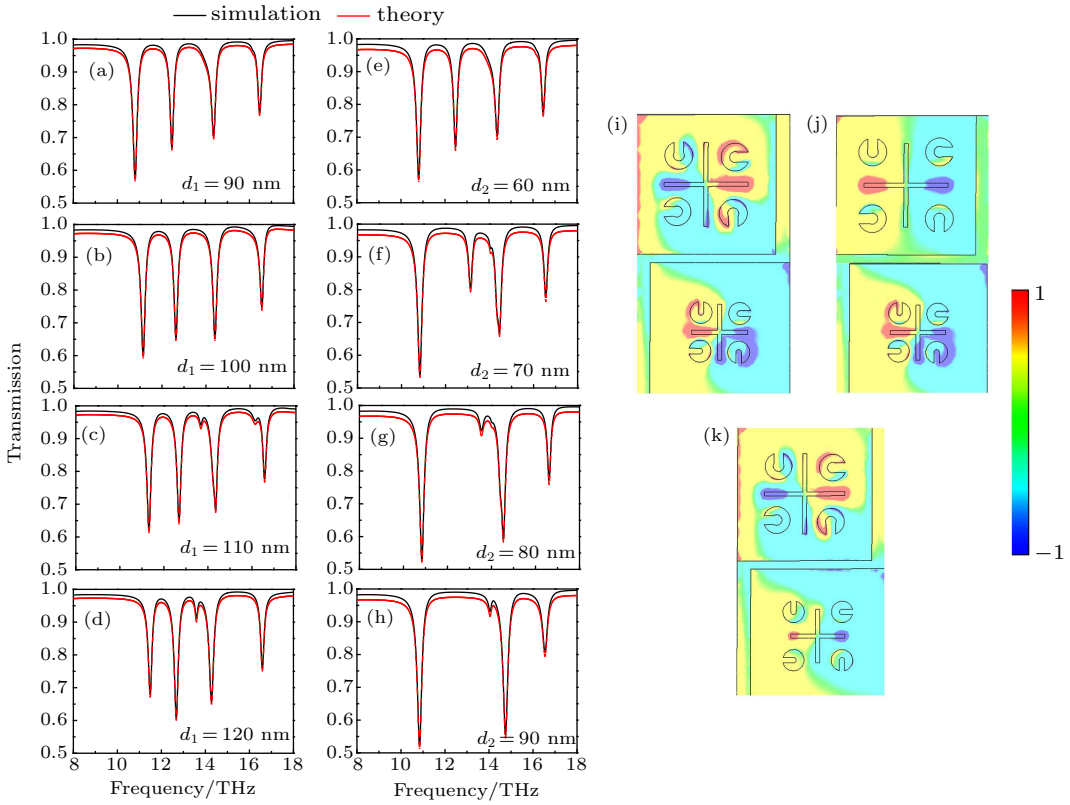


Fig. 3. Simulated transmission spectra of the proposed MM structure with different relative displacements d_1 (a)–(d) and d_2 (e)–(h), respectively. (i)–(k) The H_z distributions of combined structure at the transmission dip for different d_1 and d_2.

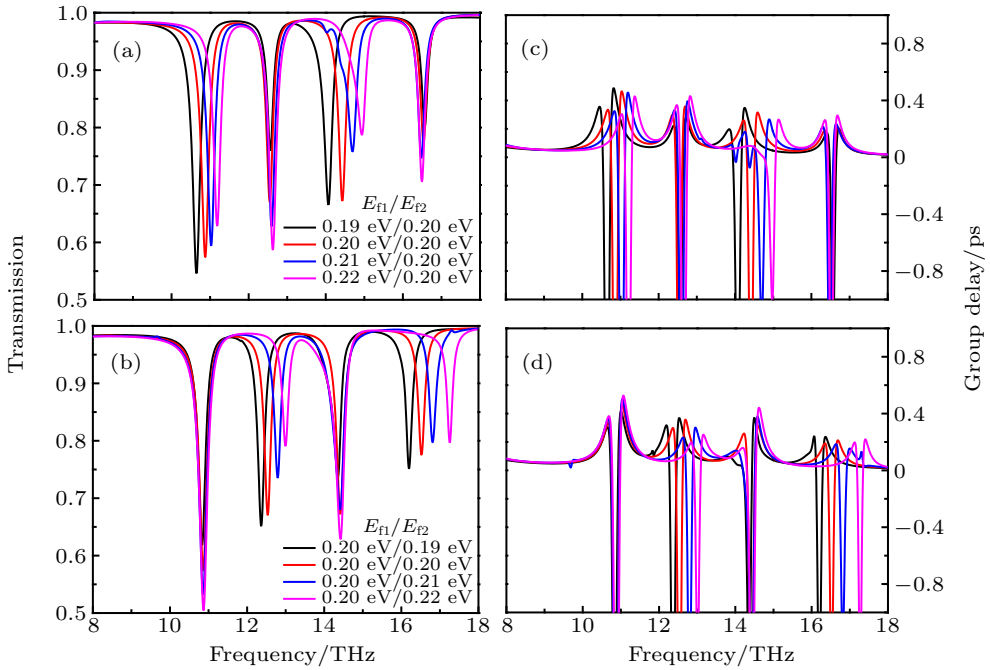


Fig. 4. Simulated transmission spectra of the proposed MM structure with different chemical potentials (a) E_{f1} and (b) E_{f2}. The corresponding group delay with different chemical potentials (c) E_{f1} and (d) E_{f2}.

Most importantly, one excellent feature of the proposed MM structure is that the polarization-insensitive transparency window can be obtained due to the center symmetry. This is highly desirable in many practical applications because the transparency window will be attenuated or even disappeared when the polarization angle is varied significantly. To demonstrate the polarization-insensitive transparency window of the designed MM structure, the transmission spectra of the pro-

posed MM structure with different polarization angles is plotted in Fig. 5. It is obviously seen that the transmission performance remains unchanged at any polarization angles α ranging from 0° to 90°, and two transmission peaks are fixed at 11.62 THz and 15.45 THz. The H_z distributions of $\alpha = 0°$ (TE mode) and $\alpha = 90°$ (TM mode) at the first resonant dip are plotted in Figs. 5(b) and 5(c), respectively. From Figs. 5(b) and 5(c), it is found that the coupling strength between two oscillators keeps unchanged except the polarity of coupled mode, proving that the performance of transmission window is not affected by the polarization mode and the resonant dip is fixed at 10.805 THz. Owing to the center symmetry, the arbitrarily polarized waves, which can be decomposed into horizontally and vertically polarized lights, can interact with the object identically. Thus, the transparency window in the proposed MM structure is polarization-independent.

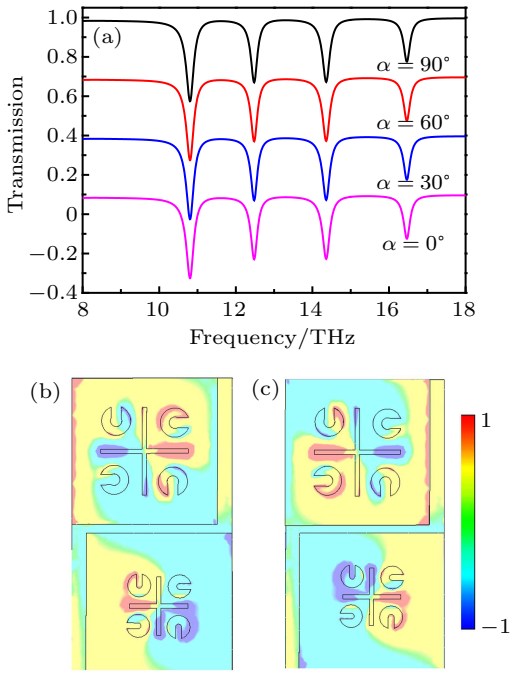


Fig. 5. (a) The transmission spectra of the proposed MM structure under different angles of the polarized wave. The H_z distributions of (b) $\alpha = 0°$ (TE mode) and (c) $\alpha = 90°$ (TM mode) at the first resonant dip.

To more deeply understand and prove the numerical results about multiple transparency windows, a theoretical mode named as a coupled harmonic oscillator system is employed to fit the simulated results. The incident E-field is set as $E_0 e^{i\omega t}$. The two strongly coupled modes in the proposed GCS are expressed as $|D_{1/2}\rangle$ and $|Q_{1/2}\rangle$, respectively. The subscripts 1 and 2 represent the large and small GCSs (G1 and G2), respectively. Based on the two oscillator modes, the field amplitude can be written as[34]

$$\begin{bmatrix} \omega - \omega_{D,1/2} + i\gamma_{Q,1/2} & \kappa_{1/2} \\ \kappa_{1/2} & \omega - \omega_{Q,1/2} + i\gamma_{D,1/2} \end{bmatrix} \begin{bmatrix} \widetilde{D}_{1/2} \\ \widetilde{Q}_{1/2} \end{bmatrix} = \begin{bmatrix} g_{1/2}\widetilde{E}_0 \\ 0 \end{bmatrix}, \tag{4}$$

where $\omega_{D,1/2}$ and $\omega_{Q,1/2}$ are the resonance frequencies of two oscillators, respectively, $\kappa_{1/2}$ is the coupling strength between two resonance structures, $g_{1/2}$ is the geometric parameters indicating the coupling strength between the oscillators, $\gamma_{D,1/2}$ and $\gamma_{Q,1/2}$ are the damping factors in two resonance structures, representing the inherent losses. Thus the transmission performance of the designed MM structure is[35]

$$T(\omega) = 1 - \left|\frac{\widetilde{D}_1}{\widetilde{E}_0}\right|^2 - \left|\frac{\widetilde{D}_2}{\widetilde{E}_0}\right|^2, \tag{5}$$

where the oscillator amplitude ($\widetilde{D}_{1/2}$) is given as[34]

$$\widetilde{D}_{1/2} = \frac{-g_{1/2}\widetilde{E}_0(\omega - \omega_{Q,1/2} + i\gamma_{Q,1/2})}{(\omega - \omega_{D,1/2} + i\gamma_{D,1/2})(\omega - \omega_{Q,1/2} + i\gamma_{Q,1/2}) - (\kappa_{1/2})^2}. \tag{6}$$

Based on Eq. (6), we can theoretically fit the simulated transmission spectrum. In Fig. 3, the theoretical transmission curve traces well with the simulated transmission results. The solid black curves represent simulated data for various d_1 and d_2, while the dotted red lines give the corresponding theoretically fitted results.

Table 1. The fitting parameters for different d_1.

Variable d_1/mm	$\omega_{D,1}/\omega_{D,2}$/THz	$\omega_{Q,1}/\omega_{Q,2}$/THz	g_1/g_2/THz	$\gamma_{D,1}/\gamma_{D,2}$/THz	$\gamma_{Q,1}/\gamma_{Q,1}$/THz	κ_1/κ_2/THz
90($d_2 = 60$)	11.28/15.87	11.46/15.56	0.11/0.03	0.28/0.09	0.15/0.05	4.89/3.45
100($d_2 = 60$)	11.51/15.81	11.65/15.68	0.16/0.03	0.25/0.07	0.13/0.04	4.42/3.45
110($d_2 = 60$)	11.72/15.83	11.79/15.62	0.18/0.03	0.24/0.05	0.12/0.03	4.03/3.45
120($d_2 = 60$)	11.95/15.79	11.83/15.60	0.21/0.03	0.21/0.03	0.10/0.01	3.72/3.45

Table 2. The fitting parameters for different d_2.

Variable d_1/mm	$\omega_{D,1}/\omega_{D,2}$/THz	$\omega_{Q,1}/\omega_{Q,2}$/THz	g_1/g_2/THz	$\gamma_{D,1}/\gamma_{D,2}$/THz	$\gamma_{Q,1}/\gamma_{Q,1}$/THz	κ_1/κ_2/THz
60($d_1 = 90$)	11.28/15.87	11.46/15.56	0.11/0.03	0.28/0.09	0.15/0.05	4.89/3.45
70($d_1 = 90$)	12.13/15.91	11.56/15.68	0.11/0.08	0.23/0.06	0.14/0.04	4.89/3.01
80($d_1 = 90$)	12.21/15.98	11.67/15.62	0.11/0.12	0.20/0.04	0.10/0.03	4.89/2.86
90($d_1 = 90$)	12.36/16.13	11.96/15.60	0.11/0.15	0.18/0.02	0.07/0.02	4.89/2.12

Also, the fitting parameters for different relative distances d_1 and d_2 are listed in Tables 1 and 2, respectively. In Table 1, the coupling strength κ_1 between two resonance modes is decreased with the increasing distance d_1, which is consistent with the different separations between two transmission dips shown in Fig. 3(a). Moreover, the relationship $\kappa_1 \gg |\gamma_{D,1} - \gamma_{D,2}|$ can be found from Table 1, which indicates that the coupling effect is in the strong coupling regime. In other words, the separation between two transmission dips is increased gradually with the increasing coupling strength between two oscillators, and further confirming the fact that the strongly coupled modes between two oscillators are the origin of multiple transparency windows, which are induced by ATS effect instead of EIT-like effect. Similarly, the parameters extracted from the fitting curves for various d_2 are given in Table 2. It is also found that the relationship $\kappa_2 \gg |\gamma_{Q,1} - \gamma_{Q,2}|$ exists, which is consistent with the relationship between κ_1 and $|\gamma_{D,1} - \gamma_{D,2}|$.

4. Conclusions

In summary, two kinds of GCSs with different sizes and element numbers are proposed to obtain the polarization-independent transparency windows in terahertz regions. The independently tunable transparency windows can be achieved by modulating the chemical potential of the corresponding GCS parts via controlling the external gate voltage. Numerical and theoretical results reveal that the transparency windows within two transmission dips are more likely caused by the ATS effect, instead of the EIT-like effect. After conducting the parametric study, the origin of multiple transparency windows is demonstrated and interpreted as the effect of two strongly coupling modes. In addition, owing to the center symmetry, the polarization-independence is realized in the proposed MM structure. The new designed complementary structure, which is based on graphene, may pave a new path for realization of multiple transparency devices, bio-sensors and switches in terahertz regimes.

References

[1] Autler S H and Townes C H 1955 *Phys. Rev.* **100** 703
[2] Boller K J, Imamoglu A and Harris S E 1991 *Phys. Rev. Lett.* **66** 2593
[3] Fleischhauer M, Imamoglu A and Marangos J P 2005 *Rev. Mod. Phys.* **77** 633
[4] He Z H, Li H J, Li B X, Chen Z Q, Xu H and Zheng M F 2016 *Opt. Lett.* **41** 5206
[5] Xu H, Li H J, He Z H, Chen Z Q, Zheng M F and Zhao M Z 2017 *Opt. Express* **25** 20780
[6] Zhan S P, Li H J, He Z H, Li B X, Chen Z Q and Xu H 2015 *Opt. Express* **23** 20313
[7] Li Q, Liu S S, Zhang X Q, Wang S and Chen T 2020 *Opt. Express* **28** 8792
[8] Wang Q, Yu L, Gao H X, Chu S W and Peng W 2019 *Opt. Express* **27** 35012
[9] Jia W, Ren P W, Tian Y C and Fan C Z 2019 *Chin. Phys. B* **28** 026102
[10] Zhu C, Tan C and Huang G 2013 *Phys. Rev. A* **87** 043813
[11] Tan C and Huang G 2014 *J. Opt. Soc. Am. B* **31** 704
[12] Zhang S, Genov D A, Wang Y, Liu M and Zhang X 2008 *Phys. Rev. Lett.* **101** 047401
[13] Li D, Huang H L, Xia H, Zeng J P, Li H J and Xie D 2018 *Results Phys.* **11** 659
[14] Zhang G Q, Lan C W, Gao R and Zhou J 2017 *J. Magn. Magn. Mater.* **436** 57
[15] Khatua S, Chang W S, Swanglap P, Olson J and Link S 2011 *Nano. Lett.* **11** 3797
[16] Chuang F T, Chen P Y, Chen T C, Chien C H and Li B J 2007 *Nanotechnology* **18** 395702
[17] Hanson G W 2008 *IEEE Trans. Anten. Propag.* **56** 747
[18] Sarkar R, Ghindani D, Devi K M, Prabhu S S, Ahmad A and Kumar G 2019 *Sci. Rep.* **9** 18068
[19] He Y W, Zhang J F, Xu W, Guo C C, Liu K, Yuan X D and Zhu Z H 2019 *Sci. Rep.* **9** 20312
[20] Bhushan S, Chauhan V S, Dixith M and Easwaran R K 2019 *Phys. Lett. A* **383** 125885
[21] Zhao S M and Zhuang P 2014 *Chin. Phys. B* **23** 054203
[22] Khazaee S and Granpayeh N 2018 *Opt. Commun.* **406** 199
[23] Huang H L, Xia H, Guo Z B, Li H J and Xie D 2018 *Opt. Commun.* **424** 163
[24] Dong Z W, Sun C, Si J G and Deng X X 2017 *Opt. Express* **25** 12251
[25] Andryieuski A and Layrinenko A V 2013 *Opt. Express* **21** 9144
[26] Hwang E H, Hu B Y K and Sarma S D 2007 *Phys. Rev. B* **76** 115434
[27] Chen J H, Jang C, Xiao S D, Ishigami M and Fuhrer M S 2008 *Nat. Nanotech.* **3** 206
[28] Huang H L, Xia H, Guo Z B, Chen Y and Li H J 2017 *Chin. Phys. B* **26** 025207
[29] Huang H L, Xia H, Guo Z B, Ding X and Li H J 2017 *Chin. Phys. Lett.* **34** 117801
[30] Tassin P, Koschny T, Kafesaki M and Soukoulis C M 2012 *Nat. Photon.* **6** 259
[31] Jian W, Bing L W, Bing X, Feng G X and Gao D Z 2014 *J. Phys. D: Appl. Phys.* **47** 325102
[32] Anisimov P M, Dowling J P and Sanders B C 2011 *Phys. Rev. Lett.* **107** 163604
[33] Ding J, Arigong B, Ren H, Zhou M, Shao J, Lu M, Chai Y, Lin Y K and Zhang H L 2015 *Sci. Rep.* **4** 6128
[34] Artar A, Yanik A A and Altug H 2011 *Nano. Lett.* **11** 1685
[35] Sun C, Dong Z, Si J and Deng X 2017 *Opt. Express* **25** 1242